A new dataset of soil Carbon and Nitrogen stocks and profiles from an instrumented Greenlandic fen designed to evaluate land-surface models

Xavier Morel[1], Birger Hansen[2], Christine Delire[1], Per Ambus[2], Mikhail Mastepanov[3,4], and Bertrand Decharme[1]

[1]CNRM UMR 3589, Meteo-France/CNRS, Toulouse, France
[2]Center for Permafrost (CENPERM), Department of Geosciences and Natural Resource Management, University of Copenhagen, Denmark
[3]Departement of Biosciences, Arctic Research Centre, Aarhus University, Roskilde, Denmark
[4] Oulanka research station, University of Oulu, Finland

Correspondence: Xavier Morel (morelxavier1@gmail.com)

Abstract. Arctic and boreal peatlands play a major role in the global carbon (C) cycle. They are particularly efficient at sequestering carbon due to their high-water content which makes primary productivity exceed decomposition rates. Though, their future in a climate-change context is quite uncertain in terms of carbon emissions and carbon sequestration. Nuuk fen site is a well-instrumented greenlandic site of particular interest for testing and validating land-surface models with

5   monitoring of soil physical variables and greenhouse gas fluxes (CH_4 and CO_2). But knowledge of soil carbon stocks and profiles is missing. This is a crucial shortcoming for a complete evaluation of models, as soil carbon is one of the primary drivers of CH_4 and CO_2 soil emissions. To tackle this issue, we measured for the first time soil carbon and nitrogen density, profiles and stocks in the Nuuk peatland, at the exact location of fluxes monitoring. Measurements were made along two transects. Measurements horizontal resolution is 5 meter, vertical resolution ranges from 5 to 10 cm. Mean soil carbon density is 50.2

10   kgC.m^{-3}. These new data are in the range of those encountered in other arctic peatlands. This new dataset can contribute to further develop joint modelisation of greenhouse gas emissions and soil carbon in land-surface models. The dataset is open-access and available at https://doi.org/10.1594/PANGAEA.909899 (Morel et al., 2019b).

1 Introduction

15   The terrestrial biosphere plays an important role in regulating atmospheric composition and climate by greenhouse gas exchanges and its capacity to act as a carbon sink. For instance, northern latitudes wetlands account for one third to half of the methane emissions from natural wetlands (Schlesinger and Bernhardt, 2013). Of all these terrestrial ecosystems, peatlands are arguably the most efficient at sequestering carbon (C) over long time scales (Loisel et al., 2014; Leifeld and Menichetti, 2018).

Peatlands are a particular type of wetlands, permanently saturated, and occur for 3 % of terrestrial surface. In these ecosystems, the anaerobic conditions due to the high water content lead to slow carbon decomposition. The accumulation rate of organic matter is hence higher than its decomposition rate. Due to their high productivity and/or slow decomposition, peatlands are consequently an important soil carbon reservoir. Their estimated carbon storage ranges between 550 and 694 GtC (Yu et al.,

5 2010; Yu, 2012). When undisturbed, these ecosystems are a net sink for atmospheric CO_2 attributed to (Jungkunst et al., 2012).

Thus, peatlands play a major role in the global carbon cycle (Harenda et al., 2018). During the Holocene, as peatland C sequestration is strongly correlated with atmospheric CO_2 concentration (Yu et al., 2011). As for the terrestrial carbon cycle, recent evidences suggest a significant shift of originally permafrost-stored carbon onto peatlands (Lindgren et al., 2018) during

10 the same period. But their future in a climate-change context is quite uncertain, in terms of carbon emissions magnitude and carbon sequestration (Yu et al., 2011).

Recent studies suggest that peatlands will remain a carbon sink in the future, although their response to global warming will switch from a negative to a positive feedback (Gallego-Sala et al., 2018). As natural carbon fluxes from and to terrestrial

15 reservoirs are annually an order of magnitude larger than perturbation from land-use change and fossil emissions (Schuur et al., 2008), large positive feedback from land biomass and soils on the atmospheric carbon pool may be triggered by a temperature increase. As peatlands organic matter accumulation rate depends not only on soil moisture but also on other factors such as soil temperature, net primary production (NPP), soil vegetation type, etc, many complex feedbacks may occur in the future. A direct feedback of climate warming on microbiological activity and, therefore, enhanced organic matter decomposition and

20 greenhouse gas emissions from soil is indeed highly probable. On the other hand, higher temperature leads to higher evapotranspiration which eventually leads to dryer conditions that may hamper decomposition despite the better temperature condition. Changes in soil moisture is also known to alter the CH_4/CO_2 ratio production.

In these regions, knowledge of carbon stocks and profiles is hence particularly important. In the last decades, a growing

25 number of sites in the arctic and boreal regions were instrumented in order to measure the greenhouse gas emissions of these ecosystems. Similarly, more and more measurements of soil carbon stocks and profiles are conducted every year. Unfortunately, although large scale soil carbon databases already exist (e.g HWSD (FAO et al., 2012) or NCSCD (Hugelius et al., 2013)), very few sites measure both the greenhouse gas fluxes together with soil carbon content (see Table 1). This is a substantial shortcoming that needs to be adressed, as carbon profiles are one of the primary drivers for CO_2 and CH_4 production

30 and emission. Moreover, for the few sites where soil carbon and greenhouse gas fluxes are available, both are quite often not measured at the same location (sometimes more than a few kilometers apart). Due to fine-scale heterogeneity (vegetation, microtopography, etc...), they may reflect completely different functioning (e.g. first datasets from Zackenberg site (Sigsgaard et al., 2007; Palmtag et al., 2015)). For a site-scale modeling point-of-view, it is then important to get fluxes data (e.g. CH_4 and CO_2) and state variable data (C stocks and profiles) as close as possible.

35

There are many challenges accompanying the joint modelisation of greenhouse gas emission and soil carbon in land-surface models. For instance, Chadburn et al. (2017) noted that models that currently get realistic soil temperature and soil carbon produce unrealistically low methane fluxes. It appears then necessary to improve the coupling of biogeochemical and physical processes of land-surface models. An example of recent attempt in this direction is the biogeochemical carbon and greenhouse

5   gas emissions model presented in Morel et al. (2019a) and embedded in the land surface model Interaction Soil-Biospheree-Atmosphère (ISBA; Noilhan and Planton (1989)). Although the biogeochemical and physical part of this model has been validated on three distinct boreal and arctic sites, the lack of soil carbon data did not allow a complete evaluation of this model. Hence, we conducted field experiments in a well-instrumented greenlandic peatland, Nuuk-fen, to collect soil carbon stocks and profiles data. Carbon sampling localisations are in the same spot as automatic chambers measuring CH_4 and CO_2 fluxes.

The aim of this paper is to present and validate a new dataset of soil carbon and nitrogen stocks and profiles from an instrumented greenlandic fen. In Section 2 we present the Kobbefjord site, in particular the fen physical characteristics and specificities. We present in Section 3 the experimental protocol and the methods of the field and laboratory studies. Section 4 presents collected data of soil bulk density, water content, soil carbon content, profiles and stocks, as well as nitrogen and

15   carbon/nitrogen (C/N) ratios. Finally, we discuss the dataset robustness and interests in Section 5. The dataset is open-access and available at https://doi.org/10.1594/PANGAEA.909899 (Morel et al., 2019b).

2   Site presentation

Nuuk Research Station is part of the Greenland Ecosystem Monitoring program, which provides detailed reports on an annual basis, dating back to 2007 for Nuuk (Nuuk Ecological Resaerch Operations - NERO - Annual reports ; Tamstorf et al. (2008)).

20   The site is well-instrumented and participates to several research programs, ranging from studying the dynamics of organisms and biological processes, the physical characteristics of marine, coastal and terrestrial environments , and climate and hydrological monitoring as well. Related data are public and open access on the Greenland Ecosystem Monitoring database repository http://data.g-e-m.dk/.

25   Located in the sub-Arctic south west of Greenland, Nuuk research station does not have any permafrost (Geng et al., 2019). It is situated in Kobbefjord (64°07'N ; 51°21'W), approximately 20 km from Nuuk. The study area consists of a drainage basin of 32 square kilometers situated at the head of a fjord. The local climate is low arctic with mean annual temperature of -1.4°C and mean annual precipitation of 752 mm (1961-90). Despite cold winter temperature, the fen never freezes at depth below $10 - 15$ cm. NERO annual reports (Tamstorf et al., 2008; Raundrup et al., 2010) show a significant variability

30   in soil texture, soil moisture, vegetation and microtopography. The studied zone, the only fen of the fjord, is surrounded by high rocks (left-top panel of Figure 1). The fen is located between the fjord and the Bade So lake. Datations of the sedimentary layer of Bade So (Larsen et al., 2017) show that the lake was under sea level until 8500 BP. Hence, the fen can not be older.

The fen is instrumented with automatic chambers and an eddy flux tower, both of partiular use for land-surface models. Soil temperatures are also monitored at different depths in the fen. There are no continuous water-measurements devices, but some isolated water table depth measurements are occasionally made throughout the year (Raundrup et al., 2010).

Due to its topographical specificity, the main input of water on this site is not from the local precipitation, but from snowmelt
5 and runoff from adjacent hills and inflow from a nearby stream located at the southern border of the fen (bottom panel of Figure 1). One key factor of this site appears to be the snowmelt date, as snowmelt water runs through the fen, leading to saturated moisture conditions during the growing season. We show that the darker areas in the center roughly correspond to the wetter areas. In these zones, the vegetation is adapted to the saturated conditions : for instance, the albedo is lower at the center than in the fen fronters, absorbing more solar radiations to compensate the colder conditions. Figure 2 shows the different vegetation
10 types encountered throughout the fen, going from green herbaceous and mosses in the outer part to aquatic plants doted with aerenchymas and *Sphagnum* in the center of the fen. Section 3.1 explains more precisely these differences in vegetation.

3 Methods and material

All the measurements were made in July 2017 alongside two transects, shown in the bottom panel of Figure 1. Each transect
15 was sampled every 5 meters, thus defining the plots $T1 - 0$, $T1 - 5$, $T1 - 10$ and so on.

The first transect (T1) roughly follows a N-S axis. The automatic chambers are situated on either side of the transect between plots $T1 - 0$ and $T1 - 20$. The second transect (T2) starts at the last automatic chamber, at the 20 meter plot of the first transect, in the middle of the fen and goes through the fen in its larger axis. The soil temperature probes can be seen between plots
20 $T2 - 30$ and $T2 - 45$.

3.1 Physical site measurement

First, we investigated the topography of the fen and the depth of the sediment layer that delimits organic and mineral soil horizons at every plot for both transects. The elevation is measured with a topographer rod. The depth of the organic-mineral interface (OMI) is measured with a rigid metallic probe. The probe is lowered into the ground until a strong resistance, char-
25 acteristic of mineral soils, is encountered.

The first transect clearly indicates an accumulation basin at the center of the fen. While the ground elevation remains approximately constant, the OMI depth strongly increases between plots $T1 - 0$ and $T1 - 30$ (Figure 3). This depression is characteristic of peatlands formation, and contributes to organic material accumulation and burial in these ecosystems. Its
30 maximal depth, of approximately 1 meter, is situated at $T1 - 30$, and roughly corresponds to the darker part of the fen surface (Figure 1) and standing water (Figures 3.a and 2.b). The OMI depth sharply increases in less than 10 meters then stays relatively stable. The plot $T1 - 40$ seems to mark the end of the fen. In this intermediate area, surface moisture conditions are

much dryer (Figure 2.d) and the vegetation does not consist of aquatic plants such as *Sphagnum* anymore. Green herbaceous and mosses became then predominant. After the exctinction of the fen, hummocky topography appears (relief characterized by mounds and depressions). The 5 meters resolution of measurement does not allow to distinguish these reliefs. The plot $T1-65$ is the shore of the nearby water stream.

The second transect starts at the 20 meter plot of the first transect ($T2-0 = T1-20$), in the middle of the fen. Until plot $T2-30$, the soil elevation and the OMI depth does not vary much. There is a peak in the OMI at $T2-45$, surrounded by 2 small depressions, while the soil elevation lowers. The end of the transect matches with the limit of the fen, and the soil elevation as the mineral layer both rises.

10 ## 3.2 Soil carbon sampling along the stransects

Soil samples were taken every 5 meter along the first transect between the plots $T1-0$ and $T1-35$, as we focus solely on the peat deposit. As the second transect fully lays in the peat deposit, we sampled its full length with a 10 meter distance between $T2-0$ and $T2-80$. Samplings were made using a manual gouge auger, with double spade grip and a cylindrical semi-open low part of 1m depth long and 4 cm diameter. The general target depth of sampling was to reach below the peat/mineral transition.
15 Samples were then extracted along the full soil core at regular intervals : every 5 cm in the top 15 centimeters, every 10 cm below.

Ideally, soil samples should be stored at a 4°C temperature before being transferred to the lab. With no fridge on the site, we used an insulated cooler in order to control at best the samples temperature. The maximum elapsed time between sample col-
20 lection and their deposit at the laboratory was 3 days. Hence, the temperature control of the samples may have not been optimal.

3.3 Soil samples handling and analysis

Soil samples ($n = 135$) were first analyzed in the Greenland Instiue of Natural Resources, located in Nuuk. For each sample, volume and mass were carefully measured following Chambers et al. (2010) method in order to determine the density of the
25 gross sample density ρ_{sample} (g.m^{-3}).

Despite a careful measurement and a method designed to limit sample compaction, we recognize that some uncertainties on the samples densities are difficult to quantify :

1. The act of measurement and the soil core extraction can compress the samples within the manual gouge auger, hence
30   modifying their structure.

2. Extracting the samples from the water-saturated soil layers without loss of water is obviously challenging, hence modifying the sample total mass. This potential loss of water can also change the available space within the soil pores, making the sample potentially more sensitive to any compaction.

3. The almost-liquid texture of the water-saturated samples makes difficult the sample volume measurement

5   Peat samples are then oven-dried at 80 °C during 48 hours to ensure constant weight was reached. Figure 4 shows samples at different depths for the soil cores $T1-10$ and $T1-25$ after drying. The samples of the $T1-10$ soil core present a well-marked color gradient indicating the different soil horizons. For example, the colour and texture of sample $10-60/65$ (taken at $60-65$ cm depth) of plot $T1-10$ is characteristic of a mineral soil and corresponds indeed to the OMI (Figure 3). On the contrary, the $T1-25$ soil core (in the center of the fen) does not have any significant gradient of color and texture, except a

10   mixed-appearence sample at $60-65$ cm depth. We show later on that these differences in color are mainly explained by soil carbon content.

After drying, we determine the mass fraction of water of each sample, noted f_{wet} (%). In order to estimate the carbon density within the soil from the mass percentage per sample dry mass, we need to know the soil bulk density, noted ρ_{bulk}, defined by

15   the dry mass per unit of total volume (Boelter, 1969; Hossain et al., 2015). The observed bulk density ρ_{bulk}^{obs} is computed as :

$$\rho_{bulk}^{obs} = \rho_{sample}(1 - f_{wet}) \tag{1}$$

Dried peat samples were then sent to the Center for Permafrost for further C and N analysis. Briefly, 10 mg portions of thoroughly mixed and finely ground sample materials was weighed into tin combustion cops for Dumas combustion (1700 °C) on an elemental analyser (CE 1110, Thermo Electron, Milan). Peat standards (Elemental Microanalysis, Okehampton, UK)

20   were included for elemental analyser mass calibration in order to obtain percentage of C and N content, noted f_C and f_N (%) respectively.

Soil carbon density ρ_C ($gC.m_{soil}^{-3}$) was then computed as :

$$\rho_C = \rho_{sample}f_C(1 - f_{wet}) = \rho_{bulk}f_C \tag{2}$$

25   Similarly, soil nitrogen density ρ_N ($gN.m_{soil}^{-3}$) was computed as :

$$\rho_N = \rho_{sample}f_N(1 - f_{wet}) = \rho_{bulk}f_N \tag{3}$$

4 Results

A total of $n = 135$ samples were collected along both transects ($n_1 = 65$ and $n_2 = 70$). For each of these samples, values of mass, volume, density, dry mass, bulk density, carbon and nitrogen content (%) and density (kg.m^{-3}), and carbon-nitrogen (C/N) ratios were measured and/or calculated. Figure 5 shows distribution histograms for all data, and descriptive statistics
5   (mean, median, upper and lower deciles) are presented in Table 2.

Figure 6 presents mean soil profiles of bulk density, water mass fraction, carbon and nitrogen content and density along both transects .

10   These soil profiles ($n = 17$) were averaged over depth for both transects, and are presented in Figure 7. As the fen depth has a substantial variability along the transects, resulting averaged profiles are noisy. For instance, samples extracted at 50 cm depth may be in a very organic soil horizon or a quasi-mineral one depending on the fen area it was extracted from. Hence, mean soil profiles do not necessarily reflect the vertical distribution of data with respect to the OMI.

15   To reduce the noise due to the OMI heterogenoity, we renormalized all the data with respect to the OMI. For a sample extracted at a depth z from a peat core with a OMI depth z_{OMI}; we define its normalized distance from OMI d_{OMI} (%) as :

$$d_{OMI} = \frac{z}{z_{OMI}} \times 100 \tag{4}$$

These normalized profiles are shown in the figure 8.

4.1 Bulk Density

20   Variation in bulk density is attributable to the relative proportion of organic and inorganic soil particles, and is a reliable indicator of the mineral or organic nature of a soil. More than 50% of the samples have a bulk density below 0.187 g.m^{-3} (Figure 5), characteristic of organic-rich material. Samples with bulk density between 0.5 and 1 $g.cm^{-3}$ corresponds to mixed organic-mineral material (Loisel et al., 2014). The higher the bulk density, the higher the mineral content. Finally, the 10% remaining samples with bulk densities higher than 0.978 $g.cm^{-3}$ (Table 2) correspond to the most mineral part of the soil, near or below
25   the OMI, as most mineral soils have bulk densities between 1.0 and 2.0 $g.cm^{-3}$ (Rezanezhad et al., 2016).

Strong vertical gradients in bulk density can be seen throughout both transects (Figure 6.a). The measured OMI depth delimits well the transition between organic and mineral material, as it should be.

30   Typical bulk density profiles in peatlands tend do show a gradual increase with depth Quinton et al. (2000) : as peat decomposition reduces the proportion of large pores by breaking down plant debris into smaller fragments (Rezanezhad et al., 2016), it increases the mass of dry material per volume of peat. Normalized mean profiles of bulk density (Figure 8.b) clearly shows this abrupt transition from mixed organic-mineral material to fully mineral soil below the OMI.

4.2 Carbon mass percentage

Figure 6 shows mass percentage of carbon in the dry samples along the two transects. They can approach 50 %, which is coherent with the proportions given in Yu (2012).

As expected, concentration of soil organic carbon in the organic layer is much higher than in the mineral horizons. High carbon
5   content in the depth of the first transect seems to indicate a carbon burial in the natural accumulation basin. We also note that the limit between the soil horizons with high carbon content and low carbon content also follows the OMI. In particular, the drop of the sedimentary layer in the first transect is clearly visible, and the variations of the mineral layer of the second transect between $T2 - 30$ and $T2 - 60$ meters as well. Normalized mean carbon content profiles (Figure 8.e) clearly shows the abrupt decrease in carbon content near the OMI. Below the OMI, carbon contents value are below 10 %, which is coherent with the
10 mineral characteristics of the soil horizons below.

4.3 Soil carbon density and soil carbon profiles

More than 70% of the soil samples have soil carbon densities comprised between 20 and 80 $kgC.m^{-3}$ (Figure 5.f). Those values are coherent with those encountered in other arctic and boreal fen and peatlands (See Chadburn et al. (2017), Fig.5). Mean local maximum of soil carbon density can reach $80 kg.m^{-3}$ (Figure 7.f). One sample has a particularly high carbon density of
15 $160 kg.m^{-3}$ (Figure 9.b). This high value may be due to a bad sample handling during the extraction or manipulation, resulting in a sample compaction that artificially increased measured bulk density.

As expected, soil carbon density matches well the measured organic-mineral interface (Figure 6.e1). The alleged carbon accumulation in the accumulation basin on the fen discussed in the previous section is confirmed, as a local maximum of soil
20 carbon density is clearly visible at the bottom of the soil plots $T1 - 25$ and $T2 - 30$ (Figure 6.a1).

Mean soil carbon density profiles are non-monotonous. In the organic horizons, SOC density increases with depth and reaches its local maximum between 60 and 80 % of the organic-mineral interface depth (Figure 8.f). Near the OMI, coherently with the abrupt decrease in carbon content and increase in bulk density discussed in the previous sections, the soil carbon
25 density decreases. Soil carbon density profiles that first increases then decreases with depth are characteristic of arctic and boreal fens (See Chadburn et al. (2017), Fig.5).

4.4 Integrated soil carbon stocks

For each peat core, total carbon stocks C_T $(kgC.m^{-2})$ were calculated by vertically integrating carbon density profiles using the trapezoïdal rule :

30 $$C_T = \sum_j (z_{j+1} - z_j) \frac{\rho_{C,j+1} + \rho_{C,j}}{2} \tag{5}$$
with z_j the sample depth and ρ_{C_j} the soil carbon density, calculated using equation (2).

Note that because of the difficulties setting the manual gouge auger much below the mineral-organic interface, the maximum sampling depth varies between the different peat cores. Hence, the integration depth also varies between peat cores. However,

5 the carbon content below this interface does not exceed 7 % except for two unusual samples (Figure 9) and we can consider that not taking into account the soil horizons below the mineral-organic interface does not underestimate much the calculated total carbon stocks.

Tables 3 and 4 presents the carbon stocks and the maximum sampling depth for each peat core along both transects. Mean

10 carbon stocks over both transects is 35.5 kg.m^{-2}. The review of Yu (2012) on high-latitude fen and peatlands gives integrated soil carbon stocks values between 58.7 and 73.4 kgC.m^{-2}, except one extra value of 113.6 kgC.m^{-2}. Those values are higher than those encountered in Nuuk. But they are computed by considering a fen depth of 1m, which is not the case here. But the Nuuk fen is quite shallow : the mean sampling depth -which is often deeper than the OMI- does not exceed 76.3 cm in both transects (Tables 3 and 4). Our soil carbon stocks measurements are then coherent and consistent with current estimates from

15 similar ecosystems.

4.5 C/N Ratios

Carbon/Nitrogen (C/N) ratios can give useful information about the nutrient content and the quality and humification degree of organic matter : a low C/N ratio is usually equivalent to a high humification level. With a mean value of 21.6, observed C/N ratio are in the range of those observed from a variety of field and laboratory studies (Bridgham et al., 1998; Rezanezhad et al.,

20 2016; Wang et al., 2015).

C/N ratios are higher in the first centimeters depth (approx. 25%), potentially indicating less microbial transformation of the peat in the upper layers (Kuhry and Vitt, 1996). In the depth of the fen, C/N ratio are lower because microorganisms slowly consume the carbon and recirculate the nitrogen, resulting in a gradual reduction of C/N values (Rydin and Jeglum, 2013). In northern regions, due to colder temperatures, the decomposition activity is slow, explaining the small difference between

25 maximal and minimal C/N values. The C/N profiles stay relatively stable throughout the depth (21.6%) and the OMI does not seem to distinguish separate zones.

Although bulk density and C/N ratio are reliable indicator for peat degradation, the lack of ash content data and isotopic measurements does not allow a quantificiation of carbon accumuluation rate nor carbon loss in the peatland (Krüger et al., 2015).

5   Discussions

Overall, this new dataset of soil bulk density, carbon and nitrgogen content, profiles and stocks is in the range of previous estimates (Yu, 2012; Loisel et al., 2014; Chimner et al., 2014).

5   As noted by Loisel et al. (2014), the accuracy of this type of measurements mostly depends on sample handling, in particular the care deployed to avoid any peat compaction. Our sample density measurements may be uncertain. On the other hand, mass carbon percentage are independent of any compression or any physical aleas. And it is known that soil carbon content and bulk density are strongly correlated. For instance, (Hossain et al., 2015) noted that bulk density ρ_{bulk}^{H} and carbon content f_C follows an exponential relationship :

10   $\rho_{bulk}^{H} = a e^{-b f_C}$ (6)

with $a = 1.5641$ and $b = 0.0631$.

Figure 9.a shows carbon content versus bulk density. The strong correlation discussed in (Hossain et al., 2015) is present ($r^2 = 0.801$, Table 5). Different type of two-parameters regressions can also be used to infer bulk densities from carbon content,

15   as shown in Table 5. Soil carbon density profiles can hence be computed with two different methods : a "direct" method, using bulk density data (see eq. 2), and an an "indirect" method by computing bulk density using carbon content via one of these functional fits. This comparison shows that our measurements of bulk densities are in the right order of magnitude. But these relationships can not capture the vertical variability of the observed soil carbon profiles. Indeed, mass percentage of carbon f_C (%C) does not encapsulate all the causes of the variability of ρ_{bulk}. Consequently, inferred carbon profiles from indirect

20   methods are deceptively flat and smooth (see Figure S1). Hence, although checking that bulk density and soil carbon content measurements follows indeed this kind of relationship provides a good indicator of the dataset quality, it is not recommended to infer soil carbon profiles from these empirical relationships.

Loisel et al. (2014) choose an arbitrary cutoff value of 0.5 g.cm^{-3} to distinguish peat and non-peat material. It also roughly corresponds to the seperation between samples with mass carbon content exceeding 15 % and the others (Figures 9.a,b,c).

25   Below this threshold (i.e. for fully organic samples), there is a linear relationship between bulk density ρ_{bulk} and soil carbon density ρ_C (Figures 9.b), indicating a rather homogeneous soil carbon content f_C for organic samples. For mixed-material and mineral samples, such relationship is not true.

The well-known water-retention capacity of peat soils (e.g. (Boelter, 1969)) is also observed in Figure 9.c, as the higher

30   values of soil-water content are found in the samples with the highest carbon content and lowest bulk densities.

Finally, when using these data for land-surface model validation, it is preferable to only use the soil carbon data corresponding to the automatic chambers area, that is the profiles from plots $T1 - 0$ to $T1 - 20$.

6 Code and data availability

All the data used to produce the tables and figures of the paper are freely available on the repository :

https://doi.org/10.1594/PANGAEA.909899 (Morel et al., 2019b)

7 Conclusions

5   In this paper, we have provided a complete description of a new dataset of current distribution of soil organic carbon storage at the Nuuk peatland. All data are in the range of previous studies (Yu et al., 2011; Yu, 2012; Loisel et al., 2014; Hossain et al., 2015). Moreover, automatic chambers fluxes measurement and carbon sampling localisations are in the same spot, making Nuuk-fen dataset an ideal candidate for evaluating ability of land surface models to reproduce both soil carbon profiles and greenhouse gas emissions at the scale of the site. It will allow in the near future a complete evaluation of the biogeochemical

10 model presented in Morel et al. (2019a). Completing this evaluation could help eventually resolve issues raised by Chadburn et al. (2017). It could also be used further validate recent devlopments in carbon and/or peatlands modules for larger scale studies, such as the specific peatland module developed by Largeron et al. (2018) or the soil carbon representation specific to fen and peatlands of Qiu et al. (2018).

Appendix A: Calculation of 95% confidence interval soil profile

15 The sampling mean most likely follows a normal distribution. Under this hypothesis, the standard error of the mean (SEM) can be calculated as $\sigma_{\overline{X}}(z) = \frac{\sigma(z)}{\sqrt{N(z)}}$ with N(z) the number of samples collected at a depth (z) and $\sigma(z)$ the standard deviation over those samples. The confidence interval at 95% is defined as $I(z) = \overline{X}(z) \pm 1.96 \times \sigma_{\overline{X}}(z)$.

Author contributions. XM, BUH, MM, CD and BD designed the field campaign. XM and BUH conducted the field work, collected and prepared the samples for analysis. PA conducted the laboratory analysis. XM, CD and BD designed the manuscript. All authors contributed

20 to the writing.

Competing interests. The authors declare that they have no conflict of interest.

Acknowledgements. This work was supported by the Acceleration of Permafrost Thaw (APT) project through BNP Paribas Foundation, grant 2014-00000004300. This work was also supported by the H2020 project CRESCENDO "Coordinated Research in Earth Systems and Climate: Experiments, kNowledge, Dissemation and Outreach", which received funding from the European Union's Horizon 2020 research

and innovation program under grant agreement 641816. Finally, the Institut Francais du Danemark (AFD) supported this work through the grant 15/2017/CSU8.2.1.

References

Boelter, D. H.: Physical Properties of Peats as Related to Degree of Decomposition1, Soil Science Society of America Journal, 33, 606, https://doi.org/10.2136/sssaj1969.03615995003300040033x, 1969.

Bridgham, S., Updegraff, K., and Pastor, J.: Carbon, Nitrogen, and Phosphorus Mineralization in Northern Wetlands, Ecology, 79, 1545–
5 1561, https://doi.org/10.1890/0012-9658(1998)079[1545:CNAPMI]2.0.CO;2, 1998.

Chadburn, S. E., Krinner, G., Porada, P., Bartsch, A., Beer, C., Belelli Marchesini, L., Boike, J., Ekici, A., Elberling, B., Friborg, T., Hugelius, G., Johansson, M., Kuhry, P., Kutzbach, L., Langer, M., Lund, M., Parmentier, F.-J. W., Peng, S., Van Huissteden, K., Wang, T., Westermann, S., Zhu, D., and Burke, E. J.: Carbon stocks and fluxes in the high latitudes: using site-level data to evaluate Earth system models, Biogeosciences, 14, 5143–5169, https://doi.org/10.5194/bg-14-5143-2017, 2017.

10 Chambers, F., Beilman, D., and Yu, Z.: Methods for determining peat humification and for quantifying peat bulk density, organic matter and carbon content for palaeostudies of climate and peatland carbon dynamics, Mires and Peat, 7, 1–10, 2010.

Chimner, R. A., Ott, C. A., Perry, C. H., and Kolka, R. K.: Developing and Evaluating Rapid Field Methods to Estimate Peat Carbon, Wetlands, 34, 1241–1246, https://doi.org/10.1007/s13157-014-0574-6, 2014.

FAO, ISRIC, ISSCAS, and JRC: Harmonized World Soil Database (version 1.2). FAO, Rome, Italy and IIASA, Laxenburg, Austria, http:
15 //webarchive.iiasa.ac.at/Research/LUC/External-World-soil-database/HTML/, 2012.

Gallego-Sala, A., Charman, D., Brewer, S., E. Page, S., Prentice, I., Friedlingstein, P., Moreton, S., J. Amesbury, M., W. Beilman, D., Björck, S., Blyakharchuk, T., Bochicchio, C., K. Booth, R., Bunbury, J., Camill, P., Carless, D., Chimner, R., Clifford, M., Cressey, E., and Zhao, Y.: Latitudinal limits to the predicted increase of the peatland carbon sink with warming, Nature Climate Change, 8, https://doi.org/10.1038/s41558-018-0271-1, 2018.

20 Geng, M. S., Christensen, J. H., and Christensen, T. R.: Potential future methane emission hot spots in Greenland, Environmental Research Letters, 14, 035 001, https://doi.org/10.1088/1748-9326/aaf34b, 2019.

Harenda, K., Lamentowicz, M., Samson, M., and Chojnicki, B.: The Role of Peatlands and Their Carbon Storage Function in the Context of Climate Change, pp. 169–187, Springer International Publishing, https://doi.org/10.1007/978-3-319-71788-3_12, 2018.

Hossain, M., Chen, W., and Zhang, Y.: Bulk density of mineral and organic soils in the Canada's arctic and sub-arctic, Information Processing
25 in Agriculture, 2, 183 – 190, https://doi.org/https://doi.org/10.1016/j.inpa.2015.09.001, 2015.

Hugelius, G., Tarnocai, C., Broll, G., Canadell, J. G., Kuhry, P., and Swanson, D. K.: The northern circumpolar soil carbon database: Spatially distributed datasets of soil coverage and soil carbon storage in the northern permafrost regions, Earth System Science Data, 5, 3–13, https://doi.org/10.5194/essd-5-3-2013, 2013.

Jammet, M., Dengel, S., Kettner, E., Parmentier, F.-J. W., Wik, M., Crill, P., and Friborg, T.: Year-round CH_4 and CO_2 flux dynamics in two
30 contrasting freshwater ecosystems of the subarctic, Biogeosciences, 14, 5189–5216, https://doi.org/10.5194/bg-14-5189-2017, 2017.

Jungkunst, H. F., Krüger, J. P., Heitkamp, F., Erasmi, S., Fiedler, S., Glatzel, S., and Lal, R.: Accounting More Precisely for Peat and Other Soil Carbon Resources, pp. 127–157, Springer Netherlands, Dordrecht, https://doi.org/10.1007/978-94-007-4159-1_7, 2012.

Krüger, J. P., Leifeld, J., Glatzel, S., Szidat, S., and Alewell, C.: Biogeochemical indicators of peatland degradation – a case study of a temperate bog in northern Germany, Biogeosciences, 12, 2861–2871, https://doi.org/10.5194/bg-12-2861-2015, 2015.

35 Kuhry, P. and Vitt, D.: Fossil Carbon/Nitrogen Ratios as a Measure of Peat Decomposition, Ecology, 77, 271, https://doi.org/10.2307/2265676, 1996.

Largeron, C., Krinner, G., Ciais, P., and Brutel-Vuilmet, C.: Implementing northern peatlands in a global land surface model: Description and evaluation in the ORCHIDEE high-latitude version model (ORC-HL-PEAT), Geoscientific Model Development, 11, 3279–3297, https://doi.org/10.5194/gmd-11-3279-2018, 2018.

Larsen, N. K., Strunk, A., Levy, L. B., Olsen, J., Bjørk, A., Lauridsen, T. L., Jeppesen, E., and Davidson, T. A.: Strong altitudinal control on the response of local glaciers to Holocene climate change in southwest Greenland, Quaternary Science Reviews, 168, 69 – 78, https://doi.org/https://doi.org/10.1016/j.quascirev.2017.05.008, 2017.

Leifeld, J. and Menichetti, L.: The underappreciated potential of peatlands in global climate change mitigation strategies, Nature Communications, 9, https://doi.org/10.1038/s41467-018-03406-6, 2018.

Lindgren, A., Hugelius, G., and Kuhry, P.: Extensive loss of past permafrost carbon but a net accumulation into present-day soils, Nature, 560, https://doi.org/10.1038/s41586-018-0371-0, 2018.

Loisel, J., Yu, Z., Beilman, D., Camill, P., Alm, J., J Amesbury, M., Anderson, D., Andersson, S., Bochicchio, C., Barber, K., Belyea, L., Bunbury, J., Chambers, F., Charman, D., Vleeschouwer, F., Fiałkiewicz-kozieł, B., Finkelstein, S., Gałka, M., Garneau, M., and Zhou, W.: A database and synthesis of northern peatland soil properties and Holocene carbon and nitrogen accumulation, The Holocene, 24, https://doi.org/10.1177/0959683614538073, 2014.

Lüers, J., Westermann, S., Piel, K., and Boike, J.: Annual CO_2 budget and seasonal CO_2 exchange signals at a high Arctic permafrost site on Spitsbergen, Svalbard archipelago, Biogeosciences, 11, 6307–6322, https://doi.org/10.5194/bg-11-6307-2014, 2014.

Morel, X., Decharme, B., Delire, C., Krinner, G., Lund, M., Hansen, B. U., and Mastepanov, M.: A New Process-Based Soil Methane Scheme: Evaluation Over Arctic Field Sites With the ISBA Land Surface Model, Journal of Advances in Modeling Earth Systems, 0, https://doi.org/10.1029/2018MS001329, 2019a.

Morel, X., Hansen, B. U., Delire, C., Ambus, P. L., Mastepanov, M., and Decharme, B.: Soil Carbon and Nitrogen stocks and profiles from an instrumented Greenlandic fen, https://doi.org/10.1594/PANGAEA.909899, 2019b.

Noilhan, J. and Planton, S.: A Simple Parameterization of Land Surface Processes for Meteorological Models, Monthly Weather Review, 117, 536–549, https://doi.org/10.1175/1520-0493(1989)117<0536:ASPOLS>2.0.CO;2, 1989.

Palmtag, J., Hugelius, G., Lashchinskiy, N., Tamstorf, M. P., Richter, A., Elberling, B., and Kuhry, P.: Storage, landscape distribution, and burial history of soil organic matter in contrasting areas of continuous permafrost, Arctic, Antarctic, and Alpine Research, 47, 71–88, https://doi.org/10.1657/aaar0014-027, 2015.

Pastukhov, A. and Kaverin, D.: Soil carbon pools in tundra and taiga ecosystems of northeastern Europe, Eurasian Soil Science, 46, 958–967, https://doi.org/10.1134/S1064229313070077, 2013.

Pirk, N., Tamstorf, M. P., Lund, M., Mastepanov, M., Pedersen, S. H., Mylius, M. R., Parmentier, F. J. W., Christiansen, H. H., and Christensen, T. R.: Snowpack fluxes of methane and carbon dioxide from high Arctic tundra, Journal of Geophysical Research: Biogeosciences, 121, 2886–2900, https://doi.org/10.1002/2016JG003486, 2016.

Pirk, N., Mastepanov, M., López-Blanco, E., Christensen, L. H., Christiansen, H. H., Hansen, B. U., Lund, M., Parmentier, F. J. W., Skov, K., and Christensen, T. R.: Toward a statistical description of methane emissions from arctic wetlands, Ambio, 46, 70–80, https://doi.org/10.1007/s13280-016-0893-3, 2017.

Qiu, C., Zhu, D., Ciais, P., Guenet, B., Krinner, G., Peng, S., Aurela, M., Bernhofer, C., Brümmer, C., Bret-Harte, S., Chu, H., Chen, J., Desai, A. R., Dušek, J., Euskirchen, E. S., Fortuniak, K., Flanagan, L. B., Friborg, T., Grygoruk, M., Gogo, S., Grünwald, T., Hansen, B. U., Holl, D., Humphreys, E., Hurkuck, M., Kiely, G., Klatt, J., Kutzbach, L., Largeron, C., Laggoun-Défarge, F., Lund, M., Lafleur, P. M., Li, X., Mammarella, I., Merbold, L., Nilsson, M. B., Olejnik, J., Ottosson-Löfvenius, M., Oechel, W., Parmentier, F.-J. W., Peichl, M., Pirk,

N., Peltola, O., Pawlak, W., Rasse, D., Rinne, J., Shaver, G., Schmid, H. P., Sottocornola, M., Steinbrecher, R., Sachs, T., Urbaniak, M., Zona, D., and Ziemblinska, K.: ORCHIDEE-PEAT (revision 4596), a model for northern peatland CO_2, water, and energy fluxes on daily to annual scales, Geoscientific Model Development, 11, 497–519, https://doi.org/10.5194/gmd-11-497-2018, 2018.

Quinton, W., Gray, D., and Marsh, P.: Subsurface drainage from hummock-covered hillslopes in the Arctic tundra, Journal of Hydrology, 237, 113–125, https://doi.org/10.1016/S0022-1694(00)00304-8, 2000.

Raundrup, K., Aastrup, P., Nyman, J., Lauridsen, T. L., Sander Johannsson, L., Henning Krogh, P., Lund, M., and Rasmussen, L. M.: NUUK BASIC: The BioBasis programme, in: Nuuk Ecological Research Operations, 3rd Annual Report, 2009, edited by Jensen, L. and Rasch, M., National Environmental Research Institute, Aarhus University, 2010.

Rezanezhad, F., S. Price, J., L. Quinton, W., Lennartz, B., Milojevic, T., and Van Cappellen, P.: Structure of peat soils and implications for water storage, flow and solute transport: A review update for geochemists, Chemical Geology, 429, https://doi.org/10.1016/j.chemgeo.2016.03.010, 2016.

Rößger, N., Wille, C., Holl, D., Göckede, M., and Kutzbach, L.: Scaling and balancing carbon dioxide fluxes in a heterogeneous tundra ecosystem of the Lena River Delta, Biogeosciences, 16, 2591–2615, https://doi.org/10.5194/bg-16-2591-2019, https://www.biogeosciences.net/16/2591/2019/, 2019.

Rydin, H. and Jeglum, J.: The biology of peatlands, second edition., Oxford University Press, 2013.

Sachs, T., Wille, C., Boike, J., and Kutzbach, L.: Environmental controls on ecosystem-scale CH_4 emission from polygonal tundra in the Lena River Delta, Siberia, Journal of Geophysical Research, 113, G00A03, https://doi.org/10.1029/2007JG000505, 2008.

Schlesinger, W. H. and Bernhardt, E. S.: Wetland Ecosystems, in: Biogeochemistry, chap. Wetland ec, pp. 233–274, Academic Press, Oxford, UK, elsevier edn., https://doi.org/10.1016/B978-0-12-385874-0.00007-8, 2013.

Schuur, E. A. G., Bockheim, J., Canadell, J. G., Euskirchen, E., Field, C. B., Goryachkin, S. V., Hagemann, S., Kuhry, P., Lafleur, P. M., Lee, H., Mazhitova, G., Nelson, F. E., Rinke, A., Romanovsky, V. E., Shiklomanov, N., Tarnocai, C., Venevsky, S., Vogel, J. G., and Zimov, S. A.: Vulnerability of Permafrost Carbon to Climate Change: Implications for the Global Carbon Cycle, BioScience, 58, 701–714, https://doi.org/10.1641/B580807, 2008.

Siewert, M., Hanisch, J., Weiss, N., Kuhry, P., C. Maximov, T., and Hugelius, G.: Comparing carbon storage of Siberian tundra and taiga permafrost ecosystems at very high spatial resolution, Journal of Geophysical Research: Biogeosciences, 120, 1973 – 1994, https://doi.org/10.1002/2015JG002999, 2015.

Siewert, M., Hugelius, G., Heim, B., and Faucherre, S.: Landscape controls and vertical variability of soil organic carbon storage in permafrost-affected soils of the Lena River Delta, Catena, 147, 725 – 741, https://doi.org/10.1016/j.catena.2016.07.048, 2016.

Sigsgaard, C., Thorsøe, K., Fugl, A., Mastepanov, M., Friborg, T., Tamstorf, M., Hansen, B., Ström, L., and Røjle Christensen, T.: Zackenberg Basic: The Climate Basis and GeoBasis programmes, in: 12th Annual Report 2006, Zackenberg Ecological Research Operations, National Environmental Research Institute, Aarhus University, 2007.

Tamstorf, M., Iversen, K., Hansen, B., Sigsgaard, C., Fruergaard, M., Andreasen, R., Mastepanov, M., Falk, J., Ström, L., and Christensen, T.: NUUK BASIC: The GeoBasis programme, in: Nuuk Ecological Research Operations, 1st Annual Report, 2007, edited by Jensen, L. and Rasch, M., National Environmental Research Institute, Aarhus University, 2008.

van der Molen, M. K., van Huissteden, J., Parmentier, F. J. W., Petrescu, A. M. R., Dolman, A. J., Maximov, T. C., Kononov, A. V., Karsanaev, S. V., and Suzdalov, D. A.: The growing season greenhouse gas balance of a continental tundra site in the Indigirka lowlands, NE Siberia, Biogeosciences, 4, 985–1003, https://doi.org/10.5194/bg-4-985-2007, 2007.

Wang, M., Moore, T. R., Talbot, J., and Riley, J. L.: The stoichiometry of carbon and nutrients in peat formation, Global Biogeochemical Cycles, 29, 113–121, https://doi.org/10.1002/2014GB005000, 2015.

Yu, Z., Loisel, J., Brosseau, D. P., Beilman, D. W., and Hunt, S. J.: Global peatland dynamics since the Last Glacial Maximum, Geophysical Research Letters, 37, https://doi.org/10.1029/2010GL043584, 2010.

5 Yu, Z., Beilman, D. W., Frolking, S., MacDonald, G. M., Roulet, N. T., Camill, P., and Charman, D. J.: Peatlands and Their Role in the Global Carbon Cycle, Eos, Transactions American Geophysical Union, 92, 97–98, https://doi.org/10.1029/2011EO120001, 2011.

Yu, Z. C.: Northern peatland carbon stocks and dynamics: a review, Biogeosciences, 9, 4071–4085, https://doi.org/10.5194/bg-9-4071-2012, 2012.
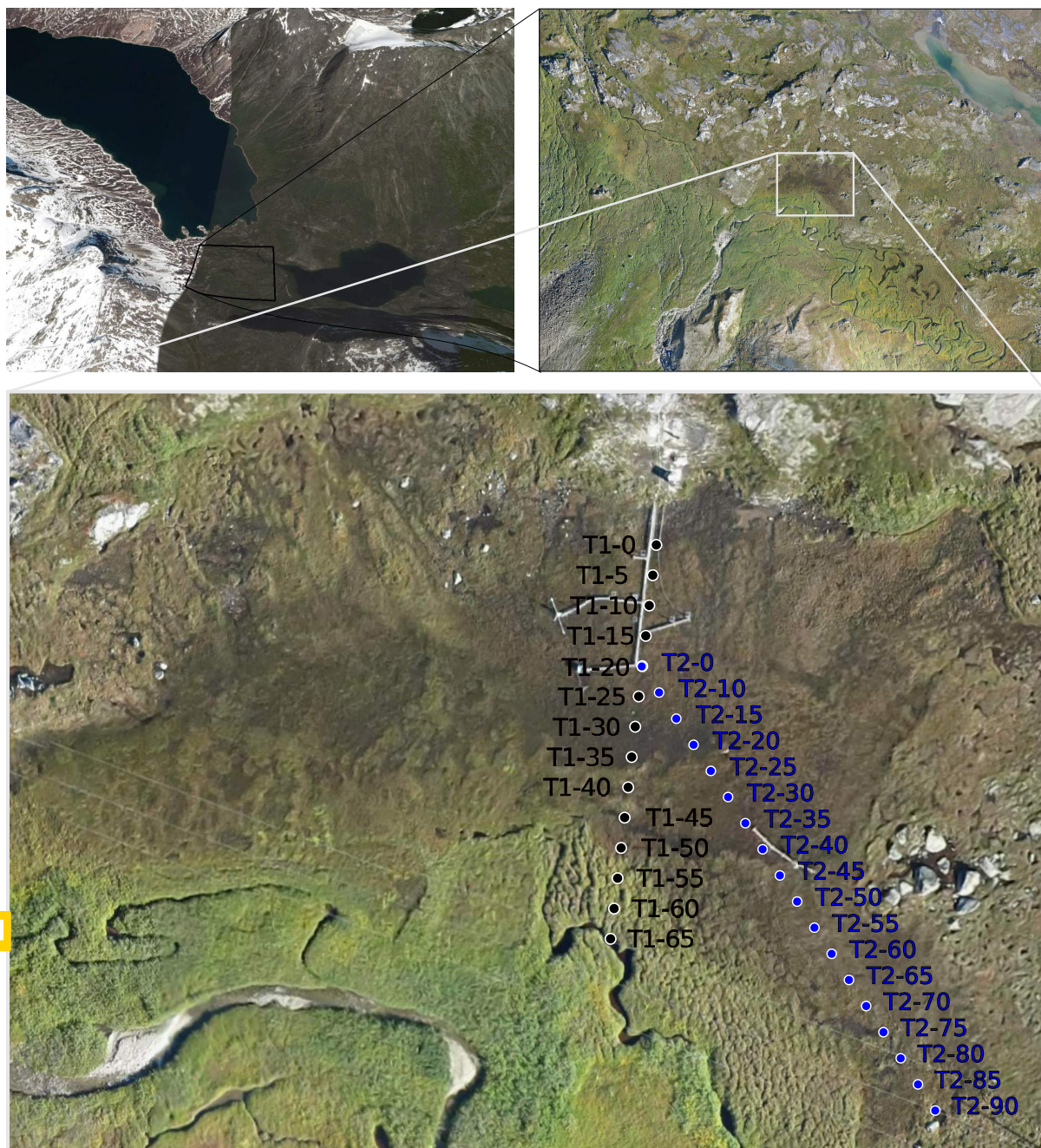
Figure 1. Left-top panel : satelite image (Google Earth© - 2009) of Kobbefjord, centered on the point 64°7'51.5"N ; 51°23'10.5"W. The black rectangle represents the sudied zone. Right-top panel : high-resolution photography (taken by a drone in 2015) of the studied zone. The white rectangle represents the fen. Bottom-panel : zoom of the fen, with the two studied transects : T1 (black circles) and T2 (blue circles).

Table 1. Short review of available carbon stocks, profiles, CO_2 and CH_4 fluxes for different sites

Site	C stock (<1m)	C profile	CO_2[1]	CH_4[1]	loc(C) = loc(GHG)[2]	Reference
Abisko	Yes[3]	Yes[4]	ET	ET	No	Jammet et al. (2017); Chadburn et al. (2017)
Bayelva	Yes[3]	Yes[4]	ET	No	No	Lüers et al. (2014); Chadburn et al. (2017)
Kytalyk	Yes[3]	Yes[4]	ET ; MC	MC	No	van der Molen et al. (2007); Chadburn et al. (2017)
Samoylov	Yes[3]	Yes[4]	ET	ET	No	Sachs et al. (2008); Siewert et al. (2015, 2016); Rößger et al. (2019)
Zackenberg	Yes[3]	Yes[4]	ET ; AC	AC	No	Pirk et al. (2016, 2017); Chadburn et al. (2017); Sigsgaard et al. (2007)
Seida	Yes	No	ET	ET	NA	Pastukhov and Kaverin (2013)
Adventdalen	No	No	AC	AC	NA	Pirk et al. (2016, 2017)
Nuuk	This study	This study	ET ; AC	AC	Yes	Pirk et al. (2016, 2017); Tamstorf et al. (2008); Raundrup et al. (2010)

(1) ET : Eddy Tower ; MC : Manual Chambers ; AC : Automatic Chambers

(2) loc(C) : Localisation of soil carbon data measurement ; loc(GHG) localisation of greenhouse gas fluxes measurement. NA = Not Announced

(3) computed via combination and harmonization of several plots (Palmtag et al., 2015; Siewert et al., 2015, 2016)

(4) computed via weighted average (Palmtag et al., 2015; Siewert et al., 2015, 2016)

Table 2. Data statistics and dispersion (mean, median, lower and upper decile)

	mean	median	lower decile	upper decile
soil sample density ρ_{sample} (g.cm^{-3})	0.940	0.898	0.445	1.528
soil bulk density ρ_{bulk}^{obs} (g.cm^{-3})	0.345	0.187	0.065	0.978
soil water content f_{wet} (%)	69.5	79.0	29.8	86.9
C/N Ratio (-)	21.6	21.0	17.1	25.9
soil carbon content f_C (%)	27.0	31.5	3.1	44.1
soil carbon density ρ_C (kgC.m^{-3})	50.2	44.8	13.1	93.3
soil nitrogen content f_N (%)	1.27	1.37	0.44	2.12
soil nitrogen density ρ_N (kgN.m^{-3})	2.37	2.25	0.59	4.17

Table 3. Carbon stocks from peat cores along the first transect

Peat core of transect 1 (m)	0	5	10	15	20	25	30	35	Mean	Std
Maximum sampling depth (cm)	55	75	65	85	95	85	75	75	76.3	12.5
Number of samples (-)	7	8	7	9	10	8	8	7	8	-
C_T (kgC.m^{-2})	31.8	52.1	37.2	29.2	46.7	55.4	40.5	34.5	40.9	9.6

Table 4. Carbon stocks from peat cores along the second transect

Peat core of transect 2 (m)	0	10	20	30	40	50	60	70	80	Mean	Std
Maximum sampling depth (cm)	85	85	85	95	65	65	65	45	70	73.3	15.4
Number of samples (-)	8	9	10	11	7	7	7	5	7	7.8	-
C_T (kgC.m^{-2})	35.4	38.4	53.4	32.3	22.2	21.6	27.3	16.6	28.6	30.7	11.0

Table 5. Statistical scores for different regressions between bulk density ρ_{bulk} and carbon content f_C

Regression type		r^2 [1]	c-rmse[2]	mae[3]	bias[4]
Hossain et al. (2015)	$\rho_{bulk}^{H} = 1.5641 \times e^{-0.0631 f_C}$	0.801	0.196	0.154	-0.10
Exponential	$\rho_{bulk}^{exp} = 0.7276 \times e^{-0.04583 f_C}$	0.760	0.222	0.147	0.07
Power	$\rho_{bulk}^{pow} = 1.8975 \times f_C^{-0.73794}$	0.817	0.164	0.117	0.032
Logarithmic	$\rho_{bulk}^{log} = -0.3281 \times \ln(f_C) + 1.31736$	0.832	0.152	0.114	$- 10^{-4}$

(1) $r^2 = \left(\dfrac{\sum_{i=1}^{n}(x_i-\overline{y})(f(x_i)-\overline{f})}{\sqrt{\sum_{i=1}^{n}(x_i-\overline{x})^2}\sqrt{\sum_{i=1}^{n}(f_i-\overline{f})^2}} \right)^2$

(2) c-rmse = $\dfrac{1}{n}\sqrt{\sum \left(x_i - \overline{x} - (f(x_i)-\overline{f}) \right)^2}$

(3) mae = $\dfrac{1}{n}\sum_{i=1}^{n}|x_i - f(x_i)|$

(4) bias = $\dfrac{1}{n}\sum_{i=1}^{n}(x_i - f(x_i))$
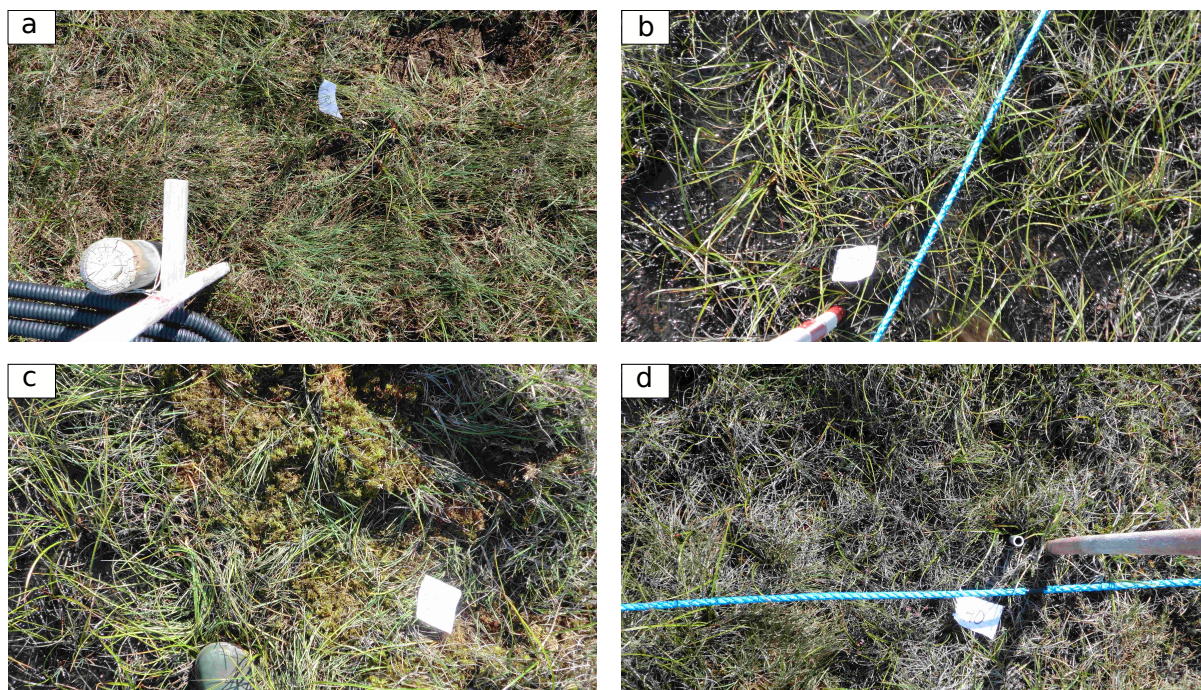
Figure 2. Soil surface photographs along the first transect at several plots. **(a)** : T1-10 ; **(b)** : T1-30 ; **(c)** : T1-35 ; **(d)** : T1-40.
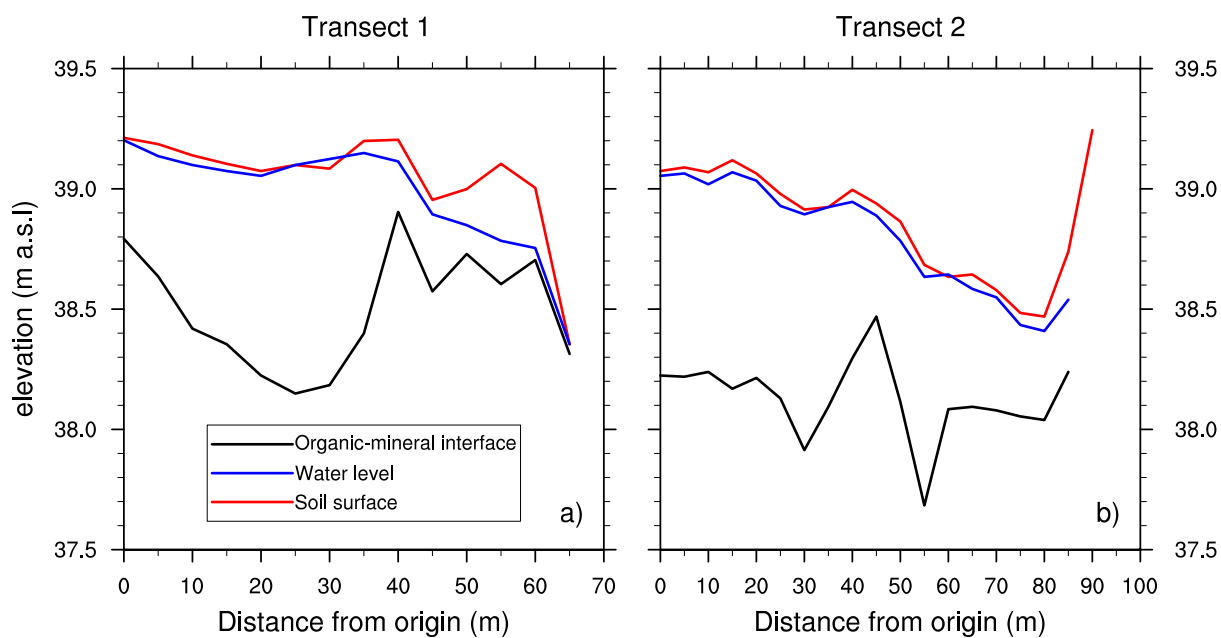
Figure 3. Topographical measurements of soil surface (red) and manual measurements of water level (blue) and organic-mineral interface (black) along both transects. Manual measurements of water level were made in July, 27th 2017.
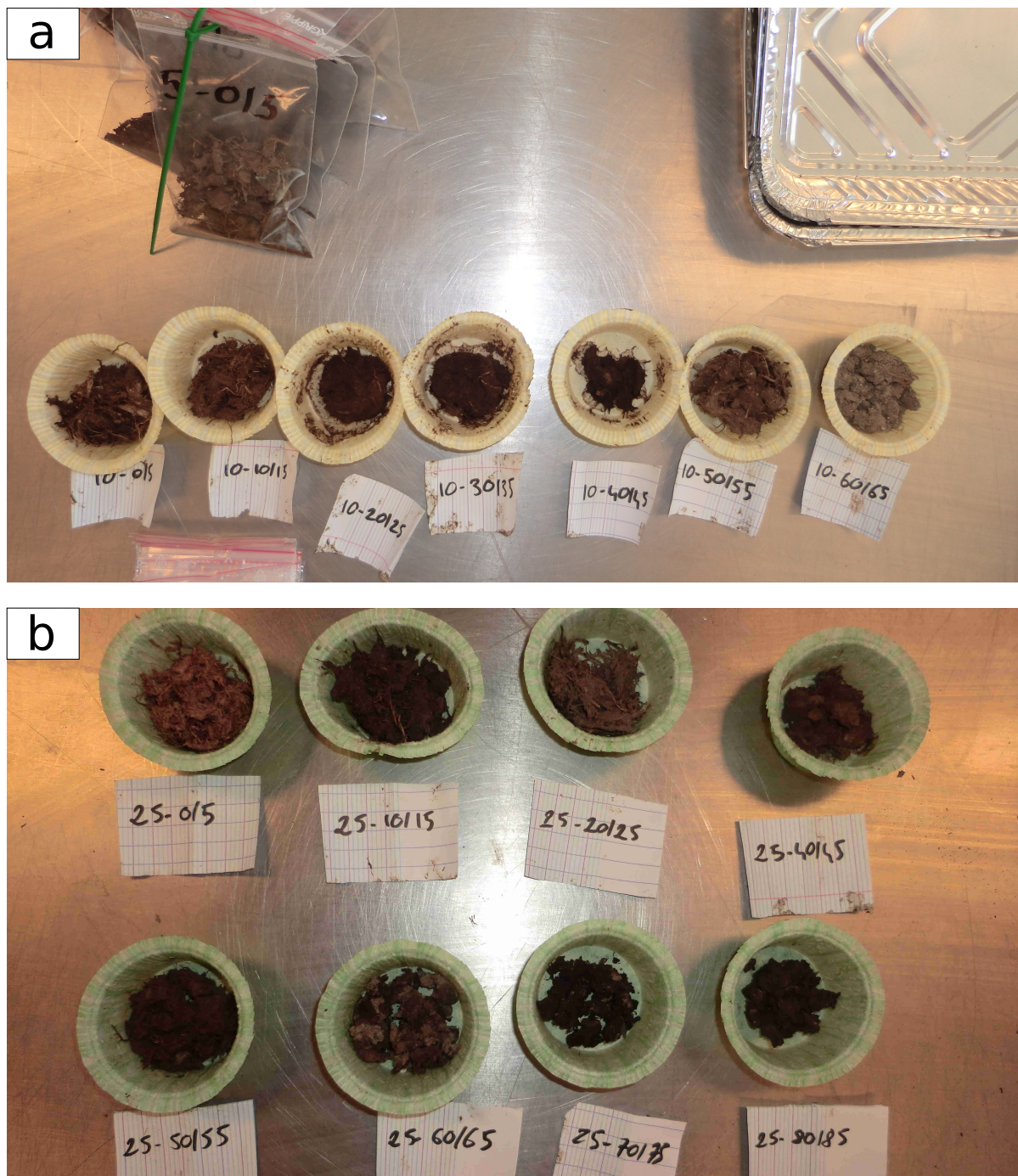
Figure 4. First transect soil samples after 48 hours of oven drying at 80 °C. Different samples depths are shown for plots **(a)** : $T1 - 10$; **(b)** : $T1 - 25$.
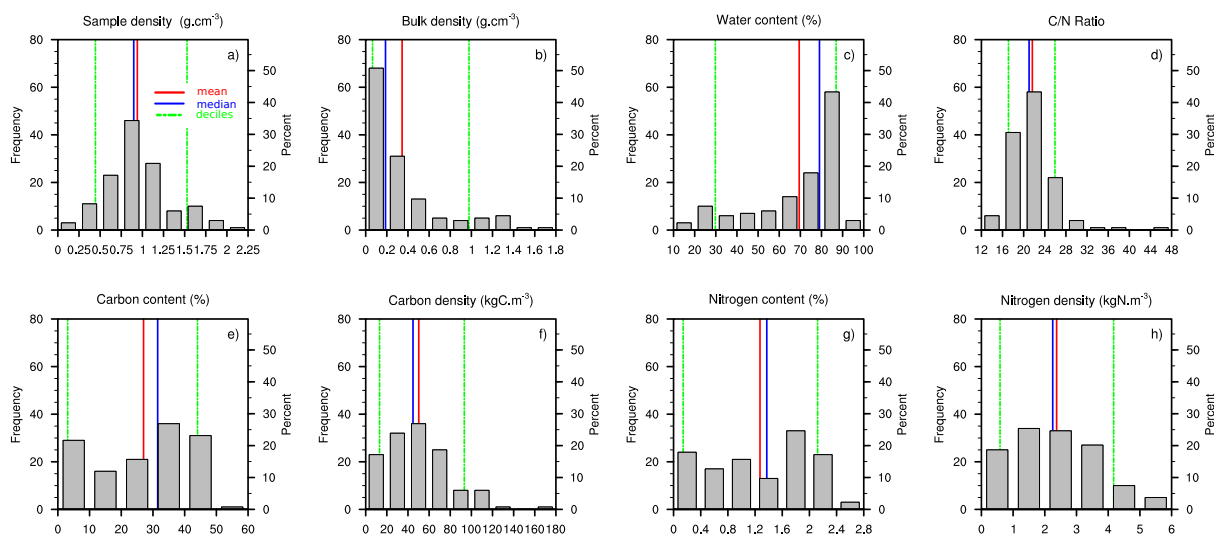
Figure 5. Distribution histograms ($n_{samples} = 135$) of **(a)** soil sample density ρ_{sample} (g.cm^{-3}) ; **(b)** soil bulk density ρ_{bulk}^{obs} (g.cm^{-3}) ; **(c)** soil water content (%) ; **(d)** C/N Ratio (-) ; **(e)** soil carbon content f_C (%) ; **(f)** soil carbon density ρ_C (kgC.m^{-3}) ; **(g)** soil nitrogen content f_N (%) ; **(h)** soil nitrogen density ρ_N (kgN.m^{-3}). Red lines represent mean values , blue lines median values , dashed green lines upper and lower deciles.
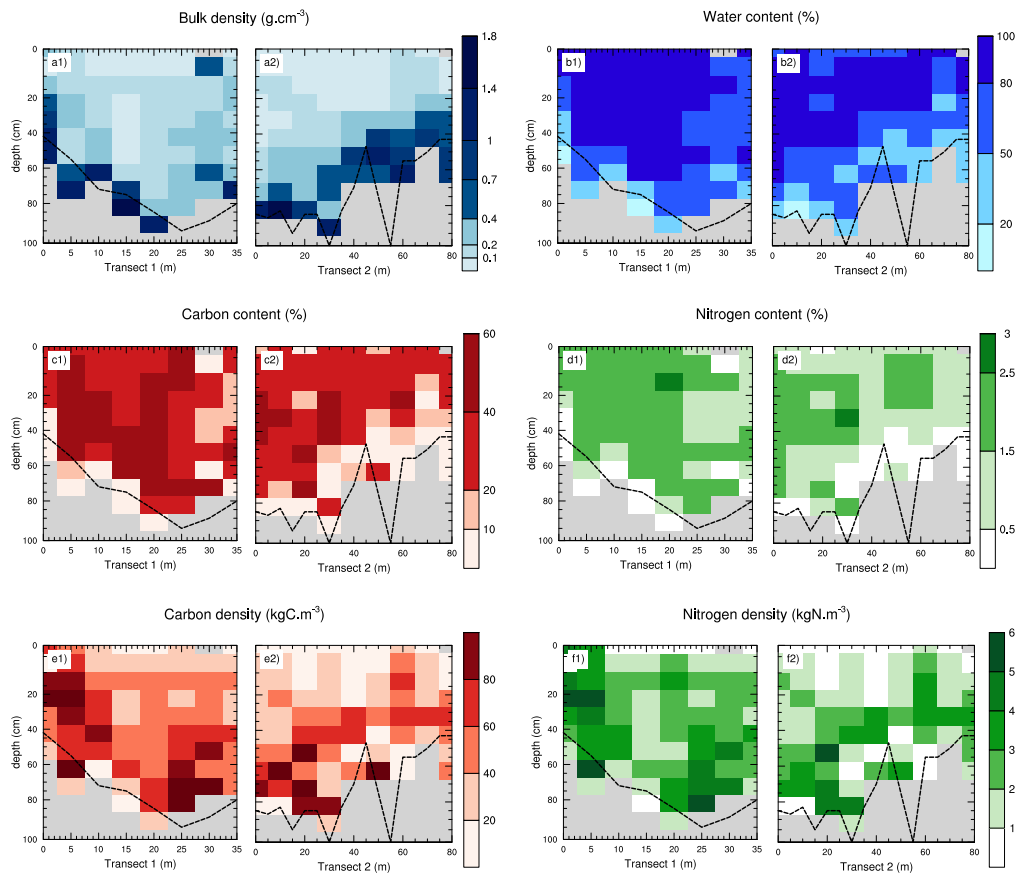
Figure 6. Soil profiles of **(a)** soil bulk density ρ_{bulk}^{obs} (g.cm^{-3}) ; **(b)** soil water content (%) ; **(c)** soil carbon content f_C (%) ; **(d)** soil nitrogen content f_N (%) ; **(e)** soil carbon density ρ_C (kgC.m^{-3}) ; **(f)** soil nitrogen density ρ_N (kgN.m^{-3}) along both transects. Dashed black line represents the measured organic-mineral interface. Grey zones indicates the absence of data (mineral soil).
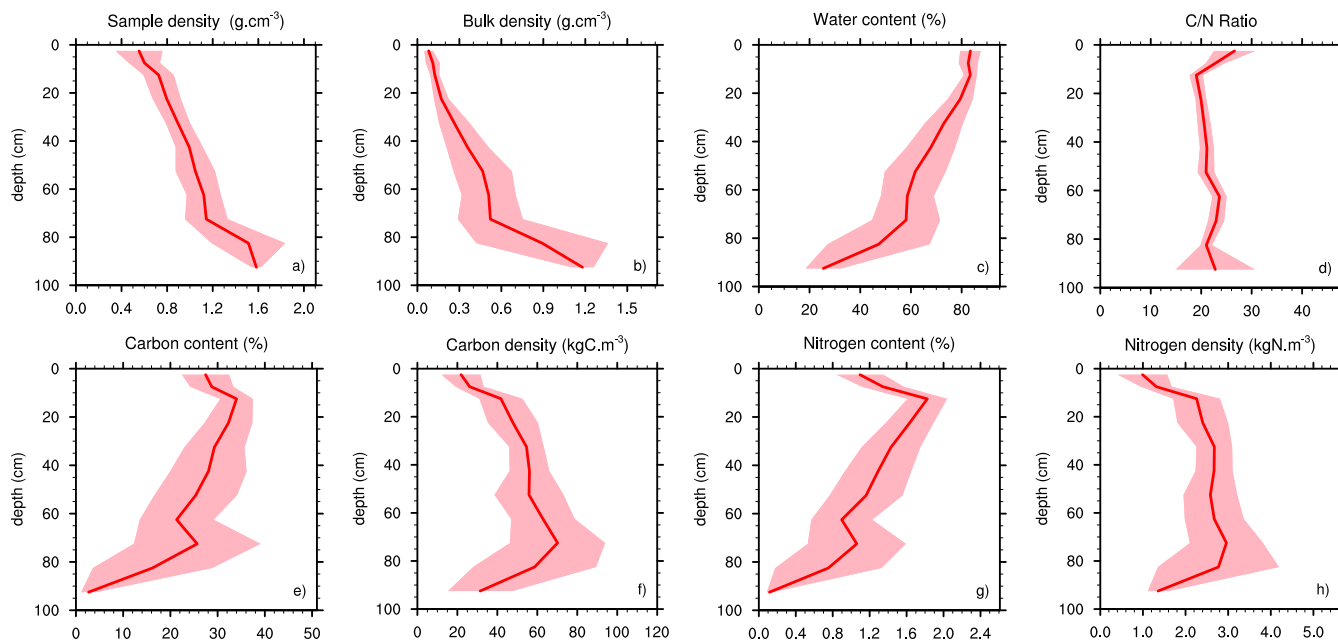
Figure 7. Mean soil profiles over both transects ($n_{samples} = 135$; $n_{profiles} = 17$) of **(a)** soil sample density ρ_{sample} (g.cm^{-3}) ; **(b)** soil bulk density ρ_{bulk}^{obs} (g.cm^{-3}) ; **(c)** soil water content (%) ; **(d)** C/N Ratio (-) ; **(e)** soil carbon content f_C (%) ; **(f)** soil carbon density ρ_C (kgC.m^{-3}) ; **(g)** soil nitrogen content f_N (%) ; **(h)** soil nitrogen density ρ_N (kgN.m^{-3}). Shaded area represents the 95% confidence interval.
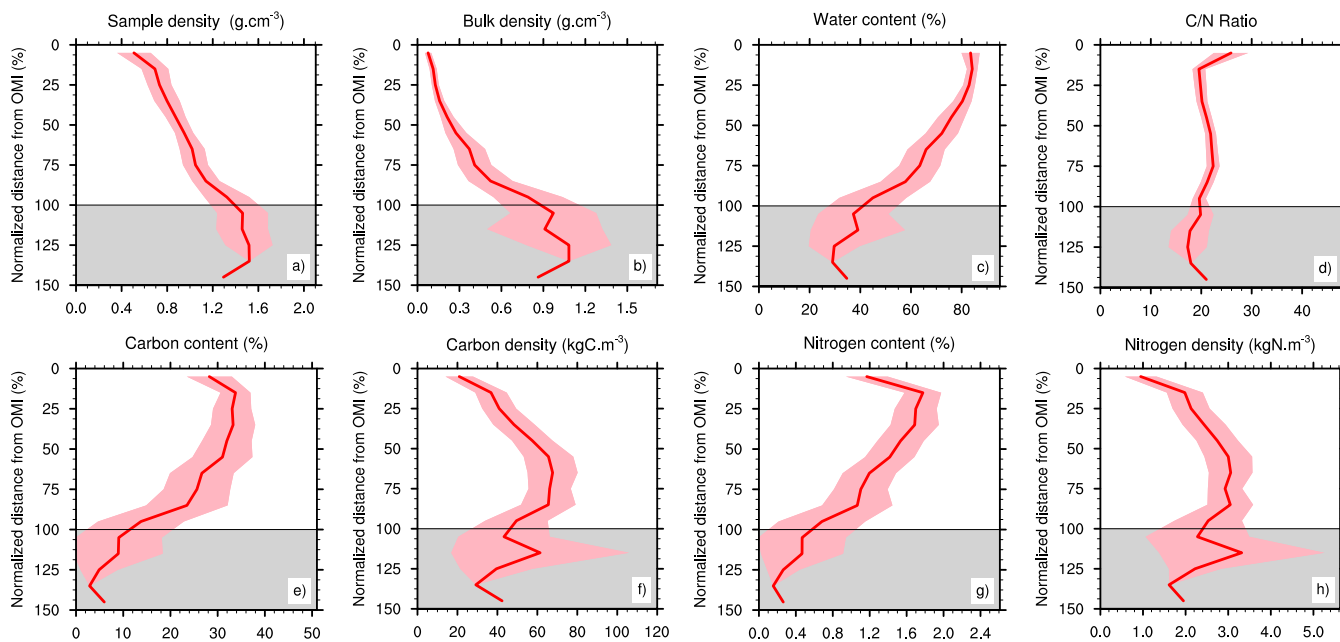
Figure 8. Same than figure 7, except profiles depth are re-normalized from organic-mineral interface. Grey area represents the zone below the OMI.
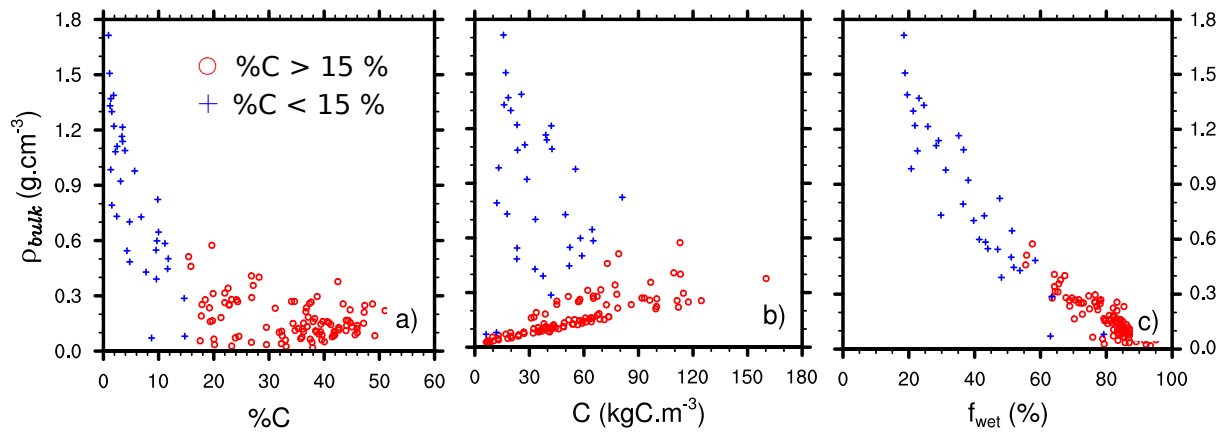
Figure 9. Scatter plots of soil bulk density ρ_{bulk}^{obs} versus **(a)** soil carbon content f_C (%) ; **(b)** soil carbon density ρ_C (kgC.m^{-3}) ; **(c)** soil water content (%) for the 135 samples. Red circles represents samples with carbon content exceeding 15 %, blue crosses less than 15 %.